frontiers in Materials

ORIGINAL RESEARCH
published: 09 September 2021
doi: 10.3389/fmats.2021.732676

Control of Magnetic Properties of Barium Ferrite Thin Films With Unusual Valence Fe

Masahiro Sakuda[1], *Hiroyasu Yamahara*[1], *Hitoshi Tabata*[1,2] *and Munetoshi Seki*[1,2]*

[1]Department of Electrical Engineering and Information Systems, Graduate School of Engineering, The University of Tokyo, Tokyo, Japan, [2]Center for Spintronics Research Network, Graduate School of Engineering, The University of Tokyo, Tokyo, Japan

Thin films of $BaFe_{1-x}M_xO_3$ (M = Hf, Zr, and Ce; $0.0 \leq x \leq 0.75$) were fabricated using pulsed laser deposition and their magnetic properties were investigated. X-ray diffraction analysis indicated that oxygen-deficient $BaFeO_x$ ($x < 3.0$) with a monoclinic structure was formed when the deposition was conducted using a non-substituted target ($x = 0.0$). The as-grown $BaFeO_x$ films were converted into fully oxidized $BaFeO_3$ with a perovskite structure by low-temperature oxidation in an ozone atmosphere. In contrast, the as-deposited films of Hf, Zr, and Ce-substituted films exhibited a perovskite structure, and their crystallinity did not change after low-temperature ozone annealing. The magnetic transition temperature T_c of the $BaFeO_3$ film was 115 K, whereas the substituted $BaFeO_3$ films showed ferromagnetic behavior even at 300 K. These results can be attributed to the weakening of the antiferromagnetic super-exchange coupling among Fe ions owing to the lattice expansion in the substituted $BaFeO_3$. In addition, the magnetization of the films was found to increase with the decreasing ionic ratio of Fe^{4+}/Fe^{3+}, suggesting that the inherent carrier-induced ferromagnetic interaction is dominant in the films.

Keywords: pulsed laser deposition, perovskite oxide, ferromagnetic oxide, barrium ferrite, Fe^{4+}-containing perovskites

OPEN ACCESS

Edited by:
Ahmad Gholizadeh, Damghan University, Iran

Reviewed by:
Saket Asthana, Indian Institute of Technology Hyderabad, India
Vipul Srivastava, Lovely Professional University, India

***Correspondence:**
Munetoshi Seki
m-seki@ee.t.u-tokyo.ac.jp

Specialty section:
This article was submitted to Thin Solid Films, a section of the journal Frontiers in Materials

Received: *29 June 2021*
Accepted: *26 August 2021*
Published: *09 September 2021*

Citation:
Sakuda M, Yamahara H, Tabata H and Seki M (2021) Control of Magnetic Properties of Barium Ferrite Thin Films With Unusual Valence Fe. Front. Mater. 8:732676. doi: 10.3389/fmats.2021.732676

INTRODUCTION

Oxide materials with unusual valence ions have attracted much attention for a long time because of their intriguing electrical and magnetic properties (Watanabe, 1957; Chen et al., 2012). In this study, we focused on perovskite-type $BaFeO_3$ with unusually high-valence Fe^{4+} ions. Barium ferrite, $BaFeO_{3-\delta}$, has various crystal structures depending on the values of the oxygen vacancy δ. For decades, a number of studies have been conducted on the crystal structures and magnetic properties of oxygen-defective $BaFeO_{3-\delta}$ (K. Mori et al., 2007, S. Mori 1966). However, owing to the large ionic radius of Ba, the synthesis of bulk $BaFeO_3$ (BFO) with a perovskite structure was not successful until recently. It has also recently been shown that fully oxidized $BaFeO_3$ can be obtained from $BaFeO_x$ ($x < 3.0$) using a low-temperature oxidation procedure (Hayashi et al., 2011). The authors reported that the obtained $BaFeO_3$ is an A-type spiral magnet with a Curie temperature (T_c) of 111 K. Likewise, Chakraverty *et al.* reported the successful growth of epitaxial $BaFeO_3$ films by pulsed laser deposition (PLD) followed by low-temperature oxidation treatment (Chakraverty et al., 2013). They reported that the M_s and T_c values for the films are 3.2 μ_B/formula unit and 115 K, respectively. Thus, the T_c value of the $BaFeO_3$ films and bulk $BaFeO_3$ is far below room temperature. Enhancing the T_c of $BaFeO_3$ is crucial from an applied viewpoint. Recently, it has been reported that the T_c of $BaFeO_3$ can be elevated by the substitution of Fe by other elements with larger ionic ratios, such as Zr and Sn

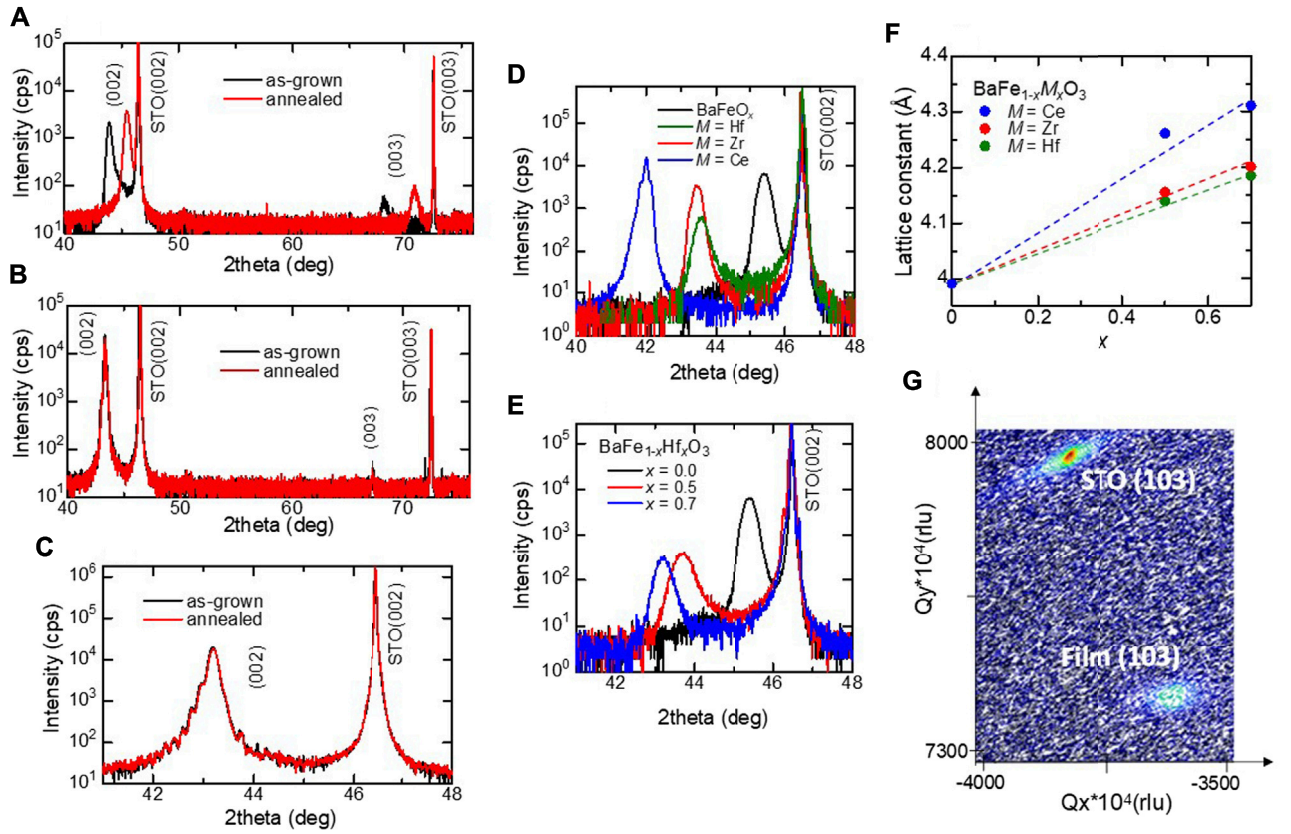

FIGURE 1 | (A) XRD 2θ–ω patterns for the $BaFeO_x$ (as-grown) and $BaFeO_3$ (annealed) films grown on the STO (001) substrate. Open and closed circles denote the peaks of $BaFeO_x$ and $BaFeO_3$, respectively. **(B)** XRD patterns of as-grown and annealed $BaFe_{0.5}Hf_{0.5}O_3$ films. **(C)** XRD patterns around (002) reflection of as-grown and annealed $BaFe_{0.5}Hf_{0.5}O_3$ films. (d) XRD patterns around the (002) reflection of $BaFe_{0.5}M_{0.5}O_3$ (M = Hf, Zr, and Ce) films. **(E)** XRD patterns around the (002) reflection of $BaFe_{1-x}Hf_xO_3$ films. **(F)** Lattice parameters as a function of the substitution level x for the BFMO films. **(G)** Reciprocal space mapping of the $BaFe_{0.5}Hf_{0.5}O_3$ thin film around the (103) Bragg reflection.

(Matsui et al., 2005; Matsui et al., 2008; Kanatani et al., 2010; Shinoda et al., 2014). However, there are few systematic studies on substituted $BaFeO_3$ in the literature. In this study, we fabricated thin films of Hf-, Zr-, and Ce-substituted $BaFeO_3$ films and investigated their magnetic properties.

EXPERIMENTAL

Thin films of $BaFe_{1-x}M_xO_3$ (BFMO) (M = Hf, Zr, and Ce; $0.0 \leq x \leq 0.75$) were fabricated by PLD followed by a low-temperature oxidation process. PLD targets were prepared via a standard solid-state reaction. A $SrTiO_3$ (STO) (001) single-crystal plate was used as the substrate. During the film deposition, the substrate temperature and oxygen pressure were maintained at 700°C and under 0.1 Pa, respectively. The as-grown films were annealed at 200 °C in an O_3 atmosphere for 3 h. The crystalline structures of the films were analyzed by X-ray diffraction (XRD) using an X-ray diffractometer (Empyrean system, Malvern Panalytical) with a Cu Kα source (λ = 0.154 nm) operated at 40 kV and 40 mA. The magnetic properties of the films were measured using a superconducting quantum interference device (MPMS, Quantum Design) over 10–300 K. To obtain detailed information about the oxidation states of the films, X-ray photoelectron spectroscopy (XPS) was conducted using an XPS system (JPS-9010 MC, JEOL) with a monochromatic Al Kα radiation source (1,486.7 eV). Optical absorption measurements were performed using a UV-Vis spectrometer (V-670, JASCO).

RESULTS AND DISCUSSION

The out-of-plane XRD patterns of the films are shown in **Figure 1A–E**. As shown in the black data in **Figure 1A**, upon using a non-substituted barium ferrite target, the resulting as-grown film comprises (001)-oriented single-crystalline $BaFeO_x$ with a pseudocubic lattice parameter of 4.12 Å. After annealing in O_3, the $BaFeO_x$ phase is converted to a (001)-oriented, single-crystalline, and cubic perovskite-type $BaFeO_3$ phase with a lattice parameter of 3.99 Å, as shown in the red data in **Figure 1A**. **Figure 1B** shows the XRD patterns of the as-grown and annealed $BaFe_{0.5}Hf_{0.5}O_3$ films. Unlike in the case of pristine $BaFeO_3$, the as-grown film shows a cubic phase, and no obvious change in the

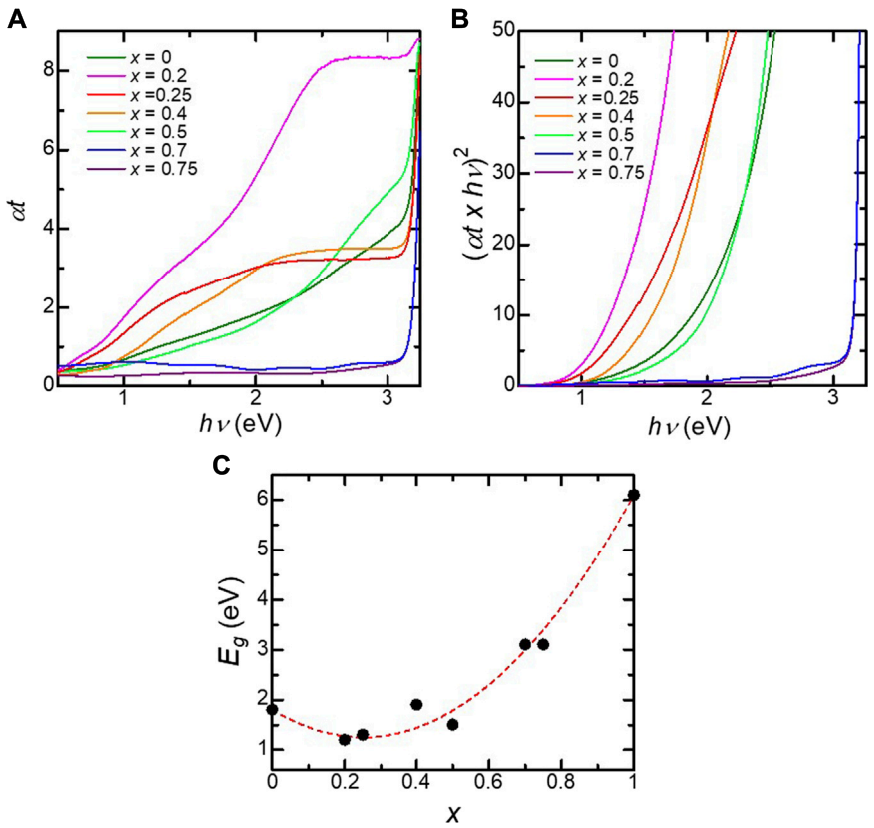

FIGURE 2 | (A) Optical absorption (αt) as a function of photon energy for the $BaFe_{1-x}Hf_xO_3$ films. **(B)** Tauc plot for the $BaFe_{1-x}Hf_xO_3$ films. **(C)** Band gap energy (E_g) as a function of the Hf content x in the $BaFe_{1-x}Hf_xO_3$ films. The value of E_g for x = 1.0 is the datum from ref. [21].

crystal structure is observed after annealing in O_3, indicating that the cubic perovskite phase is stabilized by the substitution of Hf^{4+}. This result is consistent with the fact that the Gibbs formation energy of $BaHfO_3$ is smaller than that of $BaFeO_3$ (https://materialsproject.org/materials/mp-19035/, https://materialsproject.org/materials/mp-998552/). As shown in **Figure 1C**, clear Laue fringes are observed even for the as-grown film, which suggests the high quality of the films. The lattice parameter of the as-grown and annealed films are 4.19 Å and 4.18 Å, respectively. The slightly smaller lattice parameter of the annealed film was due to oxidation. It should be noted that Ce- or Zr-substituted $BaFeO_3$ films with a cubic perovskite structure can also be fabricated by PLD without O_3 annealing as shown in **Figure 1D**. As **Figure 1E** shows, the (002) peak shifts to a lower angle with an increase in the substitution level x. This result indicates the lattice expansion of films by the substitution of M^{4+} for Fe^{4+}. **Figure 1F** shows the dependence of lattice parameters of as-grown BFMO films on the substitution level x. The lattice parameter obeys Vegard's law for M = Hf, Zr, and Ce. In addition, as clearly shown in **Figures 1D,F**, the lattice parameter increases upon increasing the ionic radius of the substituted ions [Hf^{4+} (0.78 Å), Zr^{4+} (0.84 Å), and Ce^{4+} (0.97 Å)]. These results suggest that the M^{4+} ions substitute the Fe^{4+} ions at the B-site of the perovskite structure in the films. As shown in the reciprocal space map (RSM) of **Figure 1G**, all the films are relaxed because of the large lattice mismatch (5.2–8.6%) between the film and the STO substrate.

We found that the optical properties of the BFMO films were peculiar compared to the solid-solution system. **Figure 2A** shows the optical transmission spectra of the $BaFe_{1-x}Hf_xO_3$ films. The increased absorption of $BaFeO_3$ in the visible region is attributed to O2*p*–Fe3*d* charge-transfer transitions, as suggested by first-principles calculations (Li et al., 2012; Mizumaki et al., 2015). **Figure 2A** shows the Tauc plots of the optical absorption of the $BaFe_{1-x}Hf_xO_3$ films. The bandgap energy of the BFO films is estimated to be 1.8 eV, which is close to the previously reported value (Chakraverty et al., 2013). The tails observed in the lower energy region for x = 0–0.5, in the Tauc plots can be attributed to defects in the films. As shown in **Figure 2C**, E_g exhibits a bowing behavior. The relation between the bandgap and the substitution level x can be described by the following equation based on Vegard's law (Cardona 1963; Androulidaki et al., 2006):

$$E_g(BaFe_{1-x}Hf_xO_3) = xE_g(BaHfO_3) + (1-x)E_g(BaFeO_3) - b_g x(1-x) \quad (1)$$

where b_g is the so-called bowing parameter, and $E_g(BaFe_{1-x}Hf_xO_3)$, $E_g(BaHfO_3)$, and $E_g(BaFeO_3)$ are the bandgaps of $BaFe_{1-x}Hf_xO_3$, $BaHfO_3$ Kim et al. (2017), and $BaFeO_3$, respectively. The dependence of the optical bandgap on x is well fitted with b_g = 8.7 eV, as shown by the dotted curve in **Figure 2C**.

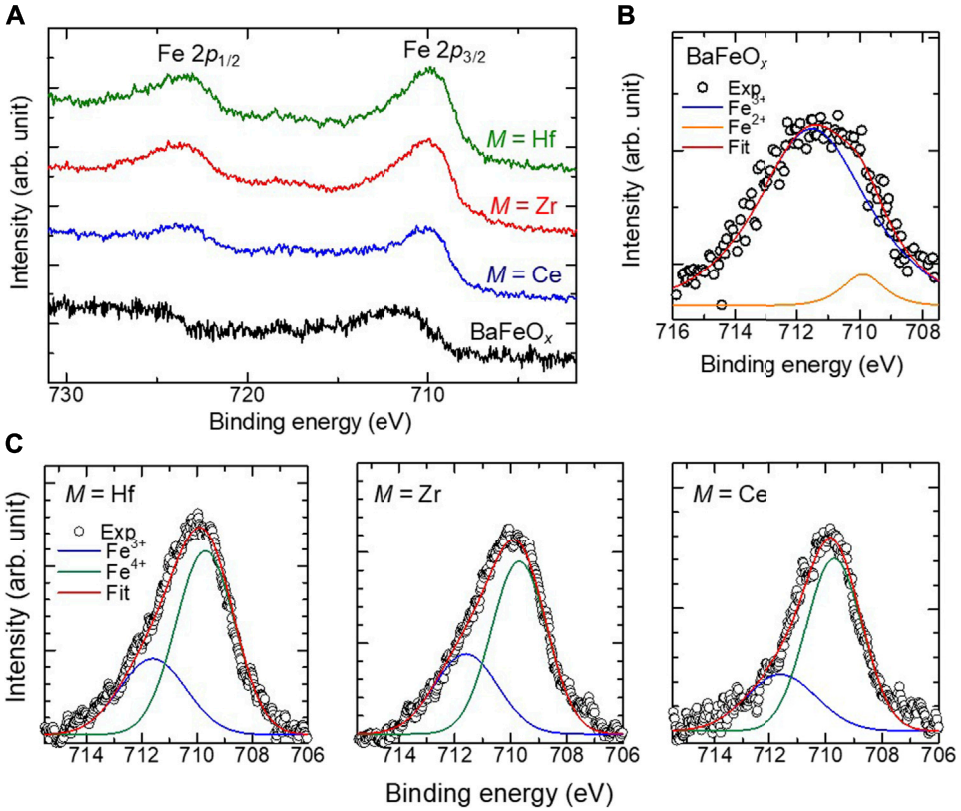

FIGURE 3 | (A) XPS spectrum of the Fe 2*p* level of the as-grown $BaFeO_x$ and $BaFeMO_3$ thin films. **(B)** A fitted XPS spectrum of the Fe level $2p_{3/2}$ level of the $BaFeO_x$ thin film. **(C)** Fitted spectra of the Fe $2p_{3/2}$ level of the $BaFeMO_3$ films.

This value is considerably larger than those reported for other alloy oxide systems such as (Ni, Mg)O Deng et al. (2012), (Fe, Mg)O Seki et al. (2014) and (Zn, Cd)O Zhu et al. (2008), suggesting a large band offset in the valence and conduction bands in the BFMO films.

XPS measurements were performed to validate the valence of the Fe ions in the films. The Fe-2p core level XPS spectra of the $BaFeO_x$ and BMFO films are shown in **Figure 3A**. The $2p_{1/2}$ and $2p_{3/2}$ peaks of the BFMO films are located at 727.0 and 709.9 eV, respectively. These peak positions are nearly the same for all BFMO films. However, the $2p_{1/2}$ and $2p_{3/2}$ peaks can be seen at 729.9 and 711.3 eV, respectively, both of which are slightly higher than those of the BFMO films, suggesting the different valence states of Fe between the $BaFeO_x$ and BFMO. As **Figure 3B** shows, when a Gaussian fitting method is used, the $2p_{3/2}$ peak of the $BaFeO_x$ film is deconvoluted into two components at 711.7 and 709.9 eV, which can be assigned to Fe^{3+} and Fe^{2+}, respectively (Temesghen and Sherwood, 2002; Li et al., 2021). The ionic ratio of Fe^{3+}/Fe^{2+} is calculated to be 13.3, indicating that most of Fe ions in the $BaFeO_x$ films are in a 3 + state. However, as shown in **Figure 3C**, the Fe 2p3/2 peak of the BFMO films consists of two major components at 711.7 and 709.6 eV, which can be assigned to Fe^{3+} and Fe^{4+}, respectively (Bocquet et al., 1992; Lombardi et al., 2019). Thus, Fe ions in the BFMO films are in the mixed valence state of Fe^{4+}/Fe^{3+}, which strongly affects the magnetic properties of the films, as discussed later. The ionic ratio of Fe^{4+}/Fe^{3+} in the annealed film (Fe^{4+}/Fe^{3+} ~ 2.0–2.5) was larger than that of the as-grown films (Fe^{4+}/Fe^{3+} ~ 1.5–1.7), suggesting the oxidation of the film after annealing in O_3.

The results of the magnetic measurements are shown in **Figure 4**. As shown in **Figure 4A**, the T_c of the BFO film is estimated to be 115 K, which agrees well with the reported value for the bulk BFO (111 K) (Hayashi et al., 2011). As shown in the inset of **Figure 4A**, the saturation magnetization of the BFO film is $\times 1.0\ 10^{-3}$ emu/cm^3 at 10 K. The magnetic properties were found to change drastically upon substitution. **Figure 4B** shows the temperature dependence of the magnetization of the BFMO films measured under a persistent magnetic field of 1 kOe. There was no significant downward trend in the magnetization of any of the films. This result provides evidence that the Curie temperature T_C of the films is well above 300 K. High temperature measurements are scheduled using the MPMS oven option to determine the value of T_C for BFMO films. As shown in **Figure 4C**, we confirmed that all the BFMO films displays ferromagnetic behaviors with coercive field of ~20–30 Oe at 300 K. **Figure 4D** shows the magnetic field *H*-dependence of the magnetization *M* of the $BaFe_{1-x}Ce_xO_3$ films at room temperature (300 K). It can be clearly seen that all these compositions exhibited room-temperature ferromagnetic behavior. This enhanced magnetization could be attributed to the lowered antiferromagnetic (AFM) coupling among Fe ions in the substituted films, as explained later. The magnetic properties

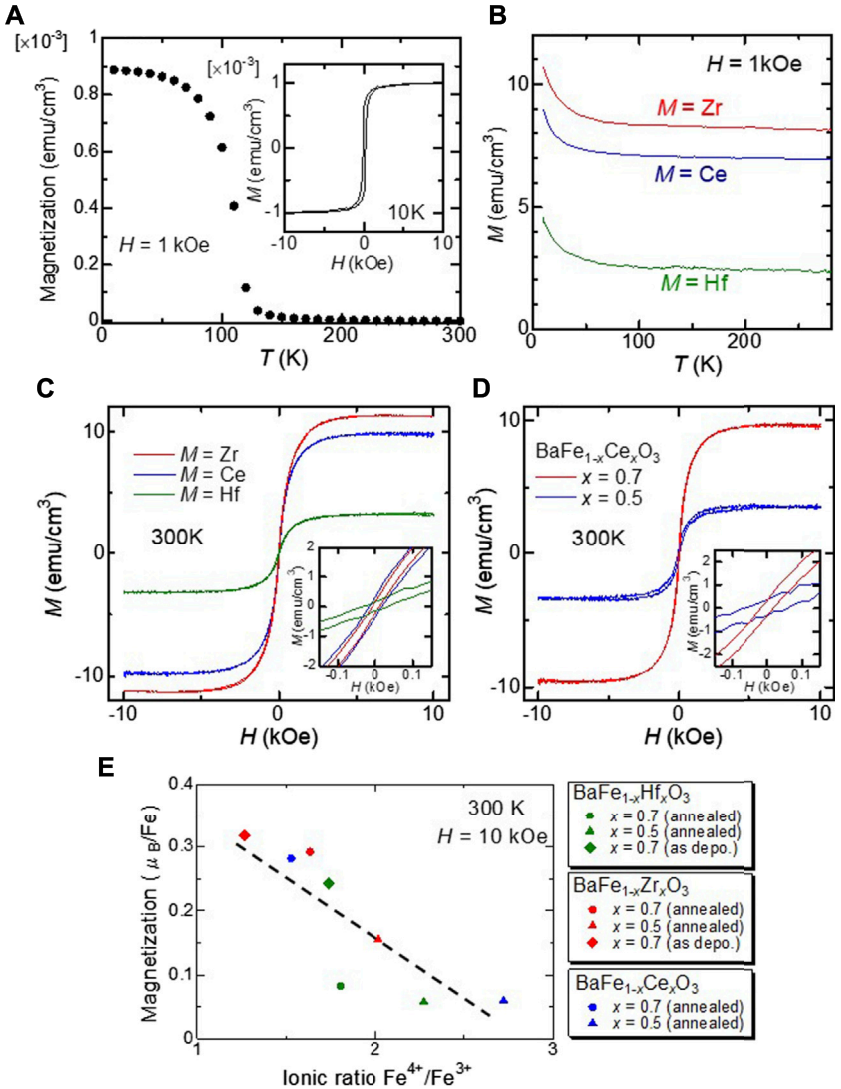

FIGURE 4 | (A) Temperature dependence of the magnetization for the $BaFeO_3$ film under a magnetic field of 10 kOe. Inset shows the magnetization as a function of magnetic field at 10 K. **(B)** Temperature dependence of the magnetization for the BFMO films under the magnetic field of one kOe. **(C)** The magnetization of the $BaFe_{0.3}M_{0.7}O_3$ films as a function of the magnetic field at 300 K. Inset shows magnified *M–H* curves of the films. **(D)** The magnetization of the $BaFe_{1-x}Ce_xO_3$ films with x = 0.5 and 0.7 as a function of the magnetic field at 300 K. Inset shows magnified *M–H* curves of the films. **(E)** Dependence of the saturation magnetization of the BFMO films on the Fe^{4+}/Fe^{3+} ratio.

of BFMO films are explained in terms of the coexistence of ferromagnetic double-exchange and antiferromagnetic super-exchange interactions. **Figure 4E** shows the dependence of the saturation magnetization on the ionic ratio Fe^{4+}/Fe^{3+}, which was calculated from the results of Gaussian fittings in the XPS analysis. As shown in **Figure 4E**, the saturation magnetization tends to decrease with an increase in the Fe^{4+}/Fe^{3+} ratio. This result indicates that the Fe^{4+}/Fe^{3+} mixed valence state enhances the ferromagnetism in the films owing to the double exchange mechanism. However, super-exchange coupling among Fe ions should also be considered. According to Harrison's relation, the super-exchange interaction J is expressed as $J \propto 1/r^{14}$, where r is the distance between Fe ions, while the double exchange interaction depends significantly less on r (Harrison 1989). Therefore, AFM coupling is drastically reduced and FM interaction becomes more prominent by substituting Fe^{4+} with M^{4+} with larger ionic radii in the films, resulting in the observed ferromagnetism at room temperature.

In summary, thin films of Hf, Zr, and Ce-substituted $BaFeO_3$ epitaxial thin films were fabricated using PLD. The highly oriented epitaxial thin films of BFMO films with a cubic perovskite structure were found to grow without annealing treatment in contrast to the pure $BaFeO_3$ film. The bandgap of the films can be varied over a wide range owing to the large bandgap bowing effect. XPS measurements revealed that the Fe ions in the BFMO films were in the mixed valence state of Fe^{4+}/Fe^{3+}. The $BaFeO_3$ film was a ferromagnet with a T_c of 115 K. On the other hand, ferromagnetic behaviors were observed at room

temperature for the BFMO films. The saturation magnetization of the BFMO films increased with an increase in the lattice parameters and ionic ratio of Fe^{4+}/Fe^{3+} in the films. The ferromagnetic behaviors of the BFMO films could be explained by the double exchange interaction and lowered AFM coupling among Fe ions caused by the substitution of Fe^{3+} by M^{4+} with a larger ionic ratio. Our findings indicate the potential of BFMO films as room-temperature ferromagnetic semiconductors.

DATA AVAILABILITY STATEMENT

The original contributions presented in the study are included in the article/supplementary material, further inquiries can be directed to the corresponding author.

AUTHOR CONTRIBUTIONS

MS: Investigation, Validation, Writing - review andamp; editing. HY: Validation, Writing - review andamp; editing. HT: Methodology, Funding acquisition, Supervision, Project administration. MS: Conceptualization, Investigation, Methodology, Validation, Writing-original draft, Funding acquisition.

FUNDING

This research was supported by the Institute for AI and Beyond at the University of Tokyo, and JSPS KAKENHI Grant Number JP18K18850.

REFERENCES

Androulidaki, M., Pelekanos, N. T., Tsagaraki, K., Dimakis, E., Iliopoulos, E., Adikimenakis, A., et al. (2006). Energy Gaps and Bowing Parameters of InAlGaN Ternary and Quaternary Alloys. *Phys. Stat. Sol. (C)* 3, 1866–1869. doi:10.1002/pssc.200565280

Bocquet, A. E., Fujimori, A., Mizokawa, T., Saitoh, T., Namatame, H., Suga, S., et al. (1992). Electronic Structure ofSrFe4+O3and Related Fe Perovskite Oxides. *Phys. Rev. B* 45, 1561–1570. doi:10.1103/physrevb.45.1561

Cardona, M. (1963). Optical Properties of the Silver and Cuprous Halides. *Phys. Rev.* 129, 69–78. doi:10.1103/physrev.129.69

Chakraverty, S., Matsuda, T., Ogawa, N., Wadati, H., Ikenaga, E., Kawasaki, M., et al. (2013). $BaFeO_3$ Cubic Single Crystalline Thin Film: A Ferromagnetic Insulator. *Appl. Phys. Lett.* 103 (1), 142416. doi:10.1063/1.4824210

Chen, W.-T., Saito, T., Hayashi, N., Takano, M., and Shimakawa, Y. (2012). Ligand-hole Localization in Oxides with Unusual Valence Fe. *Sci. Rep.* 2 (1), 449. doi:10.1038/srep00449

Deng, J., Mortazavi, M., Medhekar, N. V., and Liu, J. Z. (2012). Band Engineering of $Ni_{1-x}Mg_xO$ Alloys for Photocathodes of High Efficiency Dye-Sensitized Solar Cells. *J. Appl. Phys.* 112 (1), 123703. doi:10.1063/1.4769210

Harrison, W. A. (1989). *Electronic Structure and the Properties of Solids*. New York: Dover.

Hayashi, N., Yamamoto, T., Kageyama, H., Nishi, M., Watanabe, Y., Kawakami, T., et al. (2011). BaFeO3: A Ferromagnetic Iron Oxide. *Angew. Chem.* 123, 12755–12758. doi:10.1002/ange.201105276

Kanatani, H., Matsui, T., Hirao, N., Yamamoto, H., Baba, Y., Kume, H., et al. (2010). Improvement of Magnetic and Dielectric Properties of $BaFeO_{3-\delta}$ Thin Films by Sn Substitution A. *J. Appl. Phys.* 107 (1), 09E312. doi:10.1063/1.3360208

Kim, Y. M., Park, C., Ha, T., Kim, U., Kim, N., Shin, J., et al. (2017). High-k Perovskite Gate Oxide BaHfO3. *APL Mater.* 5 (1), 016104. doi:10.1063/1.4974864

Li, H., Yamahara, H., Tabata, H., and Seki, M. (2021). Epitaxial Thin Films of Room-Temperature Ferromagnetic Semiconductor Based on Fe_2TiO_5–$FeTi_2O_5$ Solid Solution. *Appl. Phys. Lett.* 119 (1), 022402. doi:10.1063/5.0055324

Li, Z., Laskowski, R., Iitaka, T., and Tohyama, T. (2012). First-principles Calculation of Helical Spin Order in Iron Perovskite $SrFeO_3$ and $BaFeO_3$. *Phys. Rev. B* 85 (1), 134419. doi:10.1103/physrevb.85.134419

Lombardi, J., Yang, L., Pearsall, F. A., Farahmand, N., Gai, Z., Billinge, S. J. L., et al. (2019). Stoichiometric Control over Ferroic Behavior in Ba(Ti1-xFex)O3 Nanocrystals. *Chem. Mater.* 31, 1318–1335. doi:10.1021/acs.chemmater.8b04447

Matsui, T., Sato, R., and Tsuda, H. (2008). Valence State and Spatial Distribution of Fe Ions in Ferromagnetic $Ba(Fe_{1-x}Zr_x)O_{3-\delta}$ Single-crystal Films on $SrTiO_3$ Substrates. *J. Appl. Phys.* 103 (1), 07E304. doi:10.1063/1.2836709

Matsui, T., Taketani, E., Fujimura, N., Tsuda, H., and Morii, K. (2005). Enhancement of Ferromagnetic Ordering in Dielectric $BaFe_{1-x}Zr_xO_{3-\delta}$ (x=0.5–0.8) Single-crystal Films by Pulsed Laser-Beam Deposition. *J. Appl. Phys.* 97 (1), 10M509. doi:10.1063/1.1850860

Mizumaki, M., Fujii, H., Yoshii, K., Hayashi, N., Saito, T., Shimakawa, Y., et al. (2015). Electronic Structure of BaFeO3 Studied by X-ray Spectroscopy. *Phys. Status Solidi C* 12, 818–821. doi:10.1002/pssc.201400252

Mori, K., Kamiyama, T., Kobayashi, H., Otomo, T., Nishiyama, K., Sugiyama, M., et al. (2007). Mixed Magnetic Phase in 6H-type BaFeO3−δ. *J. Appl. Cryst.* 40, s501–s505. doi:10.1107/s0021889807001653

Mori, S. (1966). Phase Transformation in Barium Orthoferrate, BaFeO3-X. *J. Am. Ceram. Soc.* 49, 600–605. doi:10.1111/j.1151-2916.1966.tb13176.x

Seki, M., Takahashi, M., Adachi, M., Yamahara, H., and Tabata, H. (2014). Fabrication and Characterization of Wüstite-Based Epitaxial Thin Films: P -type Wide-gap Oxide Semiconductors Composed of Abundant Elements. *Appl. Phys. Lett.* 105 (1), 112105. doi:10.1063/1.4896316

Shinoda, R., Iwase, A., and Matsui, T. (2014). Magneto-Dielectric Properties of Epitaxial Ba(Fe0.5Sn0.5)O3−δ Thin Films on (001) SrTiO3 Substrates by Pulsed Laser Deposition. *Mater. Trans.* 55, 637–639. doi:10.2320/matertrans.m2013429

Temesghen, W., and Sherwood, P. (2002). Analytical Utility of Valence Band X-ray Photoelectron Spectroscopy of Iron and its Oxides, with Spectral Interpretation by Cluster and Band Structure Calculations. *Anal. Bioanal. Chem.* 373, 601–608. doi:10.1007/s00216-002-1362-3

Watanabe, H. (1957). Magnetic Properties of Perovskites Containing Strontium I. Strontium-Rich Ferrites and Cobaltites. *J. Phys. Soc. Jpn.* 12, 515–522. doi:10.1143/jpsj.12.515

Zhu, Y. Z., Chen, G. D., and Ye, H. (2008). Electronic Structure and Phase Stability of MgO, ZnO, CdO, and Related Ternary Alloys. *Phys. Rev. B* 77 (1), 245209. doi:10.1103/physrevb.77.245209

Conflict of Interest: The authors declare that the research was conducted in the absence of any commercial or financial relationships that could be construed as a potential conflict of interest.

Publisher's Note: All claims expressed in this article are solely those of the authors and do not necessarily represent those of their affiliated organizations, or those of the publisher, the editors and the reviewers. Any product that may be evaluated in this article, or claim that may be made by its manufacturer, is not guaranteed or endorsed by the publisher.

Copyright © 2021 Sakuda, Yamahara, Tabata and Seki. This is an open-access article distributed under the terms of the Creative Commons Attribution License (CC BY). The use, distribution or reproduction in other forums is permitted, provided the original author(s) and the copyright owner(s) are credited and that the original publication in this journal is cited, in accordance with accepted academic practice. No use, distribution or reproduction is permitted which does not comply with these terms.